Journal of Colloid and Interface Science 581 (2021) 595–607

Contents lists available at ScienceDirect

Journal of Colloid and Interface Science

journal homepage: www.elsevier.com/locate/jcis

Mass and charge transport in highly mesostructured polyelectrolyte/electroactive-surfactant multilayer films

Esteban Piccinini [a], Graciela A. González [b], Omar Azzaroni [a,*], Fernando Battaglini [b,*]

[a] Instituto de Investigaciones Fisicoquímicas Teóricas y Aplicadas (INIFTA) –Departamento de Química, Facultad de Ciencias Exactas, Universidad Nacional de La Plata – CONICET, Suc. 4, CC 16, La Plata, Argentina
[b] INQUIMAE, Departamento de Química Inorgánica, Analítica y Química Física, Facultad de Ciencias Exactas y Naturales, Universidad de Buenos Aires – CONICET, Ciudad Universitaria, Pabellón 2 C1428EHA, Buenos Aires, Argentina

HIGHLIGHTS

- Electrochemical responsive films display well-defined mesostructure.
- The electroactive films are highly rigid and poorly hydrated.
- Film composition, redox centers concentration and electroactivity can be tuned.
- The system undergoes efficient electron transfer with negligible volume change.

GRAPHICAL ABSTRACT

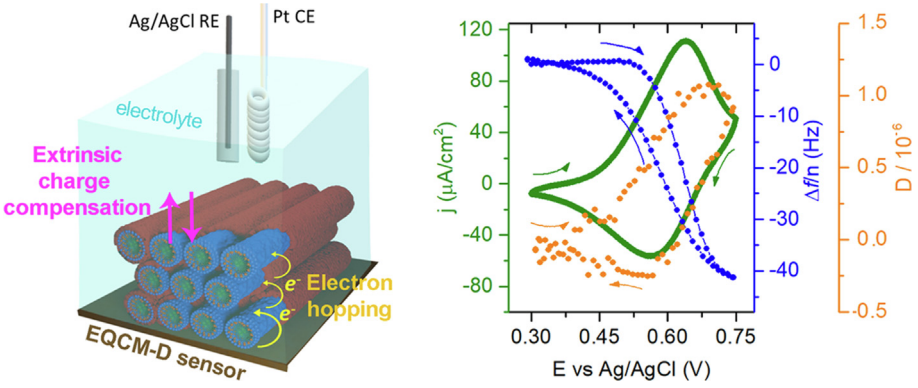

ARTICLE INFO

Article history:
Received 15 May 2020
Revised 10 July 2020
Accepted 11 July 2020
Available online 24 July 2020

Keywords:
Spatially addressed redox sites
Layer-by-layer
Mesostructured films
Electrochemical quartz crystal microbalance
Rigid film
Electron transfer
Mass transfer

ABSTRACT

Hypothesis: Dimensionally stable electroactive films displaying spatially addressed redox sites is still a challenging goal due to gel-like structure. Polyelectrolyte and surfactants can yield highly mesostructured films using simple buildup strategies as layer-by-layer. The use of redox modified surfactants is expected to introduce order and an electroactive response in thin films.
Experiments: The assembly of polyacrylic acid and different combinations of redox-modified and unmodified hexadecyltrimethylammonium bromide yields highly structured and electroactive thin films. The growth, viscoelastic properties, mass, and electron transport of these films were studied by combining electrochemical and quartz crystal balance with dissipation experiments.
Findings: Our results show that the films are highly rigid and poorly hydrated. The mass and charge transport reveal that the ingress (egress) of the counter ions during the electrochemical oxidation (reduction) is accompanied with a small amount of water, which is close to their hydration sphere. Thus, the generated mesostructured films present an efficient charge transport with negligible changes in their structures during the electron transfer process. The control over the *meso*-organization and its stability represents a promising tool in the construction of devices where the vectorial transfer of electrons, or ions, is required.

* Corresponding authors.
E-mail addresses: azzaroni@inifta.unlp.edu.ar (O. Azzaroni), battagli@qi.fcen.uba.ar (F. Battaglini).

https://doi.org/10.1016/j.jcis.2020.07.060
0021-9797/

1. Introduction

Electroactive thin films represent a crucial element in the construction of devices devoted to energy conversion, actuators, responsive materials, molecular electronics, and clinical diagnostics, among others [1–8]. In such interfaces, the precise control of the molecular components is of fundamental importance for the achievement of novel or optimized functional properties where the vectorial transfer of electrons or ions is required [9–13]. A prerequisite for the construction of mesostructured interfaces is the development of methods for integrating molecular components with strict control of their organization and alignment over the whole architecture. Research efforts on this matter are often referred to as "nanoarchitectonics", a term popularized by Ariga and coworkers [14–17]. Although there are many strategies, the construction of stable films displaying *meso*-organized functional sites with scalable and easily implementable approaches for mass production is still a challenging goal. In this context, the layer-by-layer (LbL) technique, which does not require complicated experimental setup, seems to be of great interest as it represents a versatile and straightforward approach to control the vertical composition of thin films [18–21]. Briefly, the LbL technique is based on alternate adsorption of oppositely charged nanocomponents, for instance, polycations and polyanions, and constitutes a well-established nanoconstruction method [22–25]. However, despite its intrinsic simplicity and versatility, one of the most significant limitations of LbL is its scarce control over the *meso*-organization of the components inside the film.

Exhaustive studies reported by several authors demonstrate that $(A/B)_n$ polyelectrolyte films present a low degree of organization of the components across the film [26–29]. This ill-defined *meso*- and nano-structure is evidenced by the lack of Bragg peaks when the material is characterized by X-ray reflectometry (XRR) or neutron reflectometry (NR) [30], which is explained in terms of interpenetration between polyelectrolyte layers. This effect represents a limitation to the application of the LbL technique when the precise placement and alignment of functional groups respect to the substrate is required. Different research groups explored new approaches to confer true mesoscale organization to LbL films with the purpose to overcome this issue. For example, Jonas and coworkers reported that the interpenetration between neighboring layers in multilayer assemblies can be reduced by using polyelectrolytes bearing mesogenic groups [30,31]. More recently, it has been demonstrated that the LbL assembly of polyelectrolytes and amphiphilic molecules, as mesogenic agents, is a straightforward alternative to promote *meso*-organization into these thin films [10,12,32,33]. Although the use of surfactants as structure-directing agents has been successfully employed for the construction of inorganic mesoporous films [34–36] or mesostructured surfactant-polymer "complex-salts" [37–50], its application in the buildup of well-defined mesostructures with *meso*-organized functionality using the LbL technique has been scarcely studied [10].

Since the polyelectrolyte-surfactants assemblies prepared by the complex-salts and LbL techniques can be made with the same building-blocks, it worth highlighting some essential differences between them and their resulting films: (i) In general, solution casting of polyelectrolyte-surfactant complex-salts proceeds in non-aqueous solvents (*e.g.*: chloroform, DMF), on the contrary, the LbL process takes place entirely in aqueous solutions – which is more attractive for sustainable industrial applications [6]; (ii) It was demonstrated that the polyion-surfactant LbL technique can lead to mesoscale domains with specific orientation with respect to the substrate [10,32,33], a feature that is essential for a number of applications where a vectorial transfer of electrons or ions is required; (iii) For the LbL technique, the film thickness is easily controlled with nanometric precision by the number of adsorption steps, while the complex-salts approach presents a lower control over the film thickness since the drop casting technique is typically used [45,46]; (iv) LbL allows the adsorption of an additional component (e.g., biomolecules [10], 2D materials [51], among others) in a specific location in between the polyion-surfactant layers; this feature that cannot be achieved with the complex-salts approach.

Recently, we established a supramolecular approach for the construction of layer-by-layer assemblies that leads to the generation of mesoscale-organized electroactive films [33]. These assemblies were made from the combination of the hexadecyltrimethylammonium bromide (CTA) and its ferrocenyl derivative (FcCDA), and the polyacrylic acid (PAA) (Scheme 1a). With this strategy, the density, and the *meso*-organization of the redox-centers in the film can be controlled, ranging from a circular hexagonal mesostructure to a hexagonal 2D mesostructure, depending on the composition of the surfactant mixture (Scheme 1b). The stoichiometry of redox and non-redox surfactant in the film directly correlates with the composition of the solution used in the adsorption step. Moreover, GISAXS analysis shows that these assemblies retain their structure regardless of its oxidation state, which represents an important feature when the stability of the film must be considered. The present work reports a detailed description of these attractive systems by studying the growth, composition, and viscoelastic properties of these films by quartz crystal microbalance with dissipation (QCM-D). Also, the redox state of the film was changed by cyclic voltammetry, and the charge and mass transport followed combining electrochemical and QCM-D techniques (EQCM-D). Additionally, numerical simulation allows establishing the apparent diffusion coefficient of the redox moieties and its electron transfer rate. Interestingly, these highly mesostructured films present a compact and rigid structure and a low content of water, yielding these systems as solid building block materials for devices involving energy conversion, actuators, molecular electronics, among others.

2. Experimental

2.1. Materials

2-aminoethanothiol hydrochloride (cysteamine) and hexadecyltrimethylammonium bromide (CTAB) were purchased from Sigma-Aldrich. Polyacrylic acid (M_w 5 kDa) 50 wt% solution was purchased from ACROS Organics. The electroactive cationic surfactant (ferrocenylmethyl)hexadecyldimethylammonium bromide (FcCDAB) was prepared in our laboratory following a protocol reported by Jeffrey Gold and coworkers [52,53]. All the polyelectrolyte and surfactant solutions were prepared with deionized water: 1 mg/ml PAA_{5kDa} (pH 3.7), 2 mM CTAB, 2 mM FcCDAB and CTAB-FcCDAB mixed surfactant solutions presenting a 2 mM total surfactant concentration with the following CTAB molar fractions (X^{sc}_{CTAB}): 0.9, 0.7 and 0.5. Solutions of 1 mg/ml PAA resulted in a pH value of 3.7; at this condition, the PAA is protonated around 90% [40]. The CTAB and FcCDAB solutions were prepared over the critical micelle concentration, 0.98 mM [54] and 0.17 mM [33], respectively (at 25 °C in the absence of salt).

2.2. Layer-by-layer assembly

Modification of gold surfaces with self-assembled cysteamine monolayers were done following a previously reported protocol [55]. Layer-by-layer assemblies made of polyacrylic acid and catio-

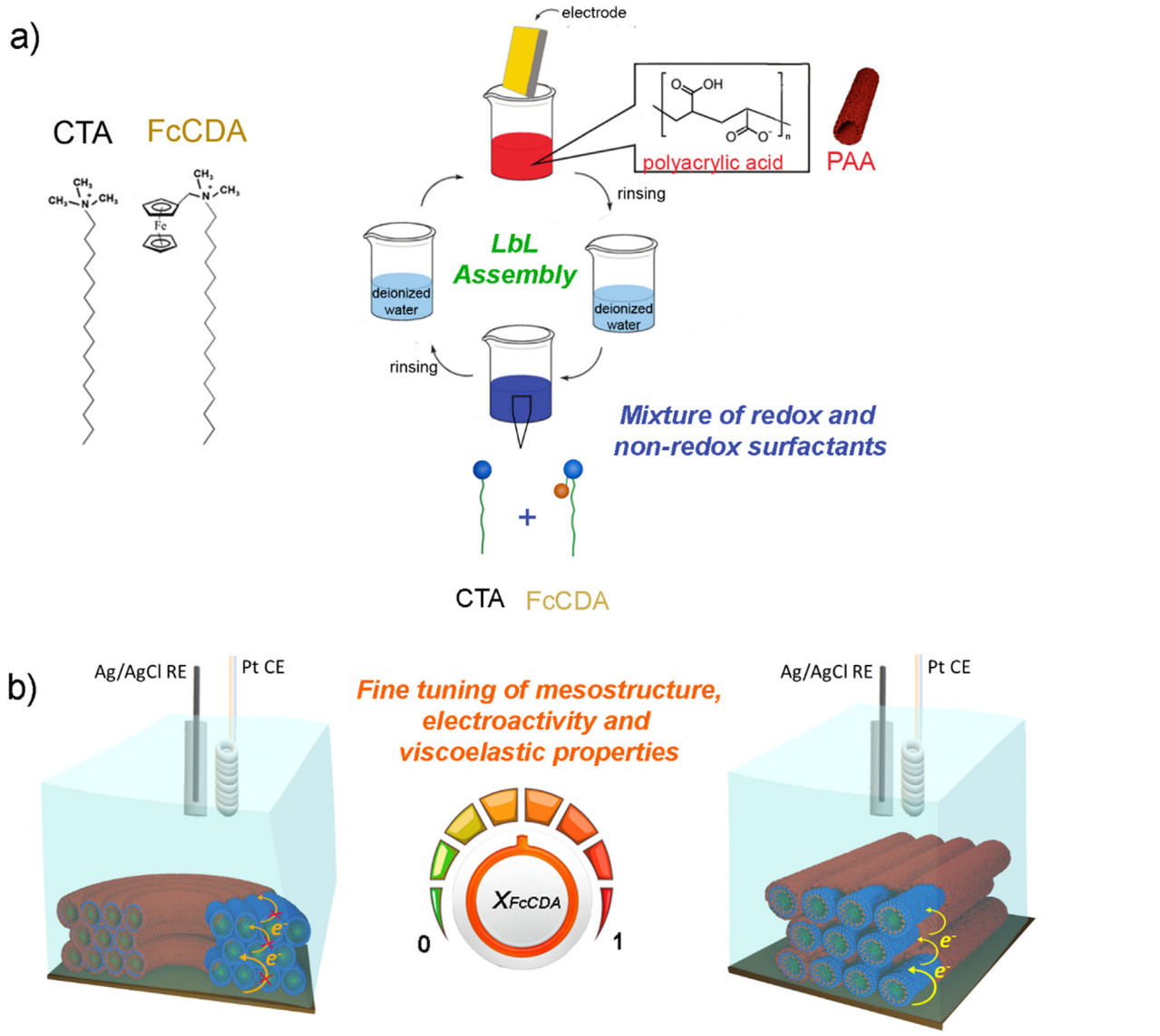

Scheme 1. a) Representation of the PAA/surfactants layer-by-layer assembly onto electrode surfaces, using the PAA (polyanion) and mixtures of the CTA and FcCDA (cationic surfactants) as building blocks. b) schematic of the resulting highly mesostructured thin-films assemblies with tailored *meso*-organization, electroactivity and viscoelastic properties.

nic surfactants were prepared on the thiol modified gold substrates (see Scheme 1a). Each adsorption step was achieved by incubating the substrate in the polyanion or surfactant solution for 10 min, followed by rinsing with deionized water for 10 min. The deposition cycle (n) is defined as the full cycle, including incubation in the polyelectrolyte, the rinse in deionized water, and the subsequent incubation in the surfactant solution followed by a water rinse. Multilayer assemblies of $(PAA/surfactants)_n$ were prepared from 1 mg/ml PAA and CTAB-FcCDAB mixed surfactant solutions with the following CTAB molar fractions (X^{sc}_{CTAB}): 1, 0.9, 0.7, 0.5 and 0. The resulting multilayer assemblies are referred as $(PAA/CTA)_n$, $(PAA/CTA_{0.9}\text{-}FcCDA_{0.1})_n$, $(PAA/CTA_{0.7}\text{-}FcCDA_{0.3})_n$, $(PAA/CTA_{0.5}\text{-}FcCDA_{0.5})_n$ y $(PAA/FcCDA)_n$, respectively.

2.3. Electrochemical measurements.

Cyclic voltammetry (CV) experiments were performed with a TEQ-03 potentiostat from NanoTeq using a three-electrode cell equipped with an Ag/AgCl (3 M NaCl) reference electrode from BASi (Indiana, USA), a platinum wire counter electrode and gold working electrodes with an active area of 0.196 cm^2 (see Scheme 1b). Unless otherwise stated, electrochemical experiments were performed at room temperature (ca. 22 °C) in 0.1 M NaCl.

2.4. Quartz-crystal microbalance with dissipation monitoring (QCM-D).

The QCM-D experiments were performed by using a Q-Sense E1 (Biolin Scientific, Sweden). For all measurements, QSX 301 gold sensors and a flow module cell were used, and the surfactant and polyelectrolyte solutions were injected manually. Frequency and dissipation were recorded at several odd overtones, and frequency shifts were normalized by division with the overtone number. Frequency and dissipation values were obtained after each adsorption step with the interface immersed in deionized water.

For the film hydration estimation, the as-prepared $(PAA/surfactant)_n$ films were dehydrated with dry nitrogen flow (0% RH) for 20 min and then exposed to a nitrogen atmosphere with a high content of water (95% RH) for 10 min. For these experiments, the Q-Sense flow cell was used.

For the simultaneous QCM-D and electrochemistry measurements (EQCM-D), a QEM 401 Qsense electrochemistry module (Biolin Scientific, Sweden) was used. This cell is equipped with a low-leak reference electrode, a platinum wire counter electrode, and the QSX 301 gold sensors as working electrodes. The EQCM-D experiments were carried out to monitor the frequency and the dissipation changes in the electroactive films during their oxidation and reduction [56–60].

The concentration of redox surfactant in the film for each system was estimated using the QCM-D results by considering the surfactant and PAA concentrations constant throughout the film. The estimation was addressed as follows: i) Based on the mass density of the film components, PAA (0.8 g/cm^3) and CTA (1.4 g/cm^3), and considering that the density of the surfactant FcCDA is equal to that of the CTA, the bulk density of the film (ρ_{film}) was estimated: $\rho_{film} = \frac{\Gamma_{surf}*\rho_{CTA}+\Gamma_{PAA}*\rho_{PAA}}{\Gamma_{total}}$. ii) The thickness of the films (d) was calculated as $d = \Gamma_{total}/\rho_{film}$. iii) Since the Sauerbrey equation is a good approximation for our films, the surfactant surface coverage (Γ_{surf}) are obtained by QCM-D and CTA:FcCDA ratio in the assemblies can be assumed to be equal to that of the solution (X^{sc}_{FcCTA}) [33]. Therefore, the concentration of FcCDA in the film is $C^{film}_{FcCTA} = \Gamma_{surf} * X^{sc}_{FcCTA}/d$.

The experimental noise for the liquid QCM-D experiments was typically below 2 ng/cm^2, and $-\Delta D/\Delta f$ was lower than 0.2×10^{-6}-Hz^{-1} during the whole layer-by-layer construction. Therefore, it is expected surface mass estimation error below 5% by using the Sauerbrey equation.

2.5. Numerical model.

Finite-element software (Comsol Multiphysics 3.4) was used to simulate the cyclic voltammetry experiments and the concentration profiles. The software was executed in a PC Intel (R) Core (TM) I5-3330 CPU@3.00 GHz – 8 GB RAM – 64-bit Operating System, resolving the model with 43,499 degrees of freedom and 9080 nodes, the mesh was refined close to the electrode where 7330 nodes were used. The experimental system was modeled solving Poisson and Fick equations using the finite-element software previously described. The space dimension was set to 2D, and the boundary conditions are an infinite modified plane electrode with a polyelectrolyte-surfactant film immersed in a buffer solution. The thickness of the film and redox surfactant concentration are according to experimental measurements. Charge propagation within the film was described by a diffusion coefficient D_e equivalent electron hopping propagation [48,61]. The generated current is calculated by the Butler-Volmer equation:

$$\frac{j}{F} = k_0\left[C_O\exp\left(\frac{-\alpha F}{RT}(E-E_{eq}\right) - C_R\exp\left(\frac{(1-\alpha)F}{RT}(E-E_{eq}\right)\right] \qquad (1)$$

where C_R and C_O are the concentration on the working electrode surface of the osmium reduced and the oxidized species, respectively; k_0 is the standard electron transfer rate constant; E is the applied potential, and E_{eq} is the equilibrium electrode potential. k_0 is determined from the adjustment of the model to experimental cyclic voltammograms in order to reproduce peak high and peak separation at different scan rates.

The model describes the general situation of an immobilized redox mediator in a layer at the electrode surface. The charge was calculated from cyclic voltammograms, whereas the value reported in Table 1 was used as redox surfactant concentration. From these values, a thickness of 57 nm was estimated. The rate of the electron hopping process was set to an equivalent diffusion coefficient of 4×10^{-12} cm^2 s^{-1}, and the scan rate was according to experimental conditions.

3. Results

3.1. Film growth, viscoelasticity, and hydration

The layer-by-layer adsorption of PAA and surfactants was monitored by QCM-D on gold surfaces modified with cysteamine. Fig. 1a) shows the frequency changes, $\Delta f/n$, after the adsorption of each component for the assembly of 14 layers using different proportions of mixed surfactants (molar fraction of FcCDA in solution: 0, 0.1, 0.3, 0.5 and 1). For all the assemblies prepared in this work, we obtained that the relationship between the dissipation and the normalized frequency changes ($-\Delta D/\Delta f$) is less than 0.2×10^{-6} Hz^{-1} (Fig. 1b) which indicates that the use of the Sauerbrey equation is a good approximation [62,63]. The mass surface coverage, Γ, (right axis of Fig. 1a) was estimated from Δf using the Sauerbrey equation (described in the experimental section). The adsorbed mass is larger as we increase the proportion of FcCDA. For example, for 7 bilayers, the assemblies $(PAA/CTA)_7$ showed a surface coating of 9.8 μg cm^{-2}, while for $(PAA/FcCDA)_7$, it was 75.4 μg cm^{-2}. As this increase in adsorbed mass is not only due to the difference in the molecular weight of each surfactant (M_W FcCDA = 470.5 and M_W CTA = 284.5 g/mol), it is inferred that a greater number of moles of surfactant and polyelectrolyte are adsorbed as the proportion of FcCDA in solution is increased. These results could be explained in terms of the self-assembling tendency of each surfactant, which is related to its critical micellar concentration (CMC). In general, the lower the value of CMC, the greater the tendency to self-assemble. In the absence of salt at 25 °C, the CMCs are 0.17 mM and 0.98 mM for FcCDA and CTA, respectively [54]. In all cases, the assemblies exhibited a supralinear growth. Moreover, the $-8\Delta D/\Delta f$ sharply decreases as FcCDA is introduced, evidencing an increase in the rigidity of the films (Table 1).

The hydration of PAA and surfactant assemblies was also studied. For this, the assemblies of 7 deposition cycles were dehydrated with dry nitrogen (0% RH) for 20 min and then exposed to a nitrogen atmosphere with a high content of water (95% RH) for 10 min. The changes in frequency and dissipation were monitored throughout the experiment (Fig. 2a). Interestingly, the films adsorbed meager amounts of water (less than 15%, Fig. 2b) compared with previously reported layer-by-layer assemblies made of polyanions and polycations (between 30 and 70%) [62,64]. Also,

Table 1
Values for Γ_{PAA}, Γ_{surf}, X^{film}_{PAA}, X^{film}_{surf}, C^{film}_{FcCDA} and -ΔD/Δf as a function of the molar fraction of FcCDA in solution after 7 bilayers.[1]

X^{sc}_{FcCDA}	Γ_{PAA}(μg/cm^2)	Γ_{surf}(μg/cm^2)	X^{film}_{PAA}	X^{film}_{surf}	C^{film}_{FcCDA}(mM)	$-8\Delta D/\Delta f$ ($\times 10^{-6}$ Hz^{-1})
0	5.93	3.55	0.87	0.13	0	0.089
0.1	4.50	4.95	0.79	0.21	188	0.01
0.3	8.80	9.65	0.81	0.19	502	0.015
0.5	7.45	13.3	0.75	0.25	923	0.01
1	17.9	46.6	0.71	0.29	1500	0.0010

[1] Surface mass estimation error is less than 5%.

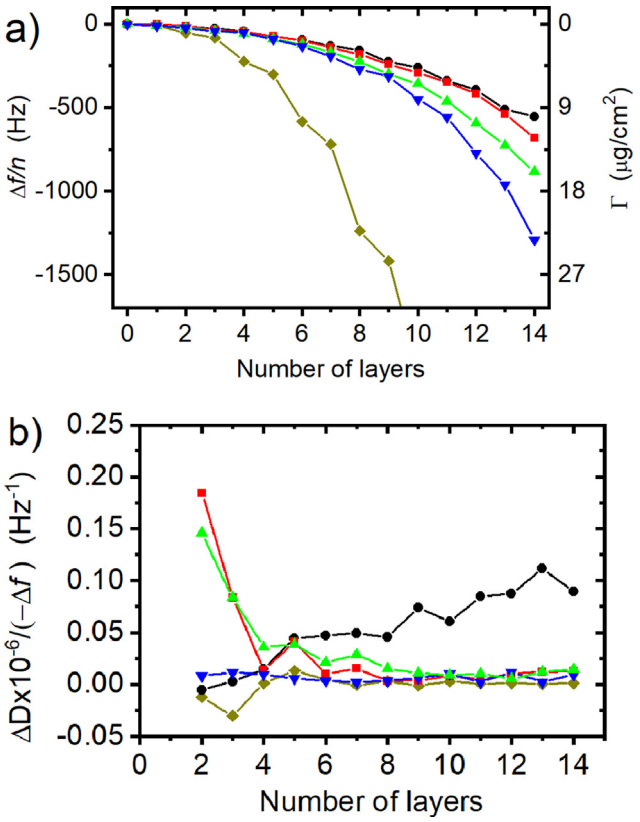

Fig. 1. a) Frequency change as a function of the number of layers for polyacrylic acid and different CTAB:FcCDAB ratios. The surface mass (Γ) was obtained using the conversion factor 17.7 ng Hz^{-1} cm^{-2}. b) Viscoelastic properties of the assemblies. The values of frequency and dissipation correspond to the 3rd overtone. (●) $(PAA\_CTA)_n$; (■) $(PAA\_CTA_{0.9}\text{-}FcCDA_{0.1})_n$; (▲) $(PAA\_CTA_{0.7}\text{-}FcCDA_{0.3})_n$; (▼) $(PAA\_CTA_{0.5}\text{-}FcCDA_{0.5})_n$; (♦) $(PAA\_FcCDA)_n$.

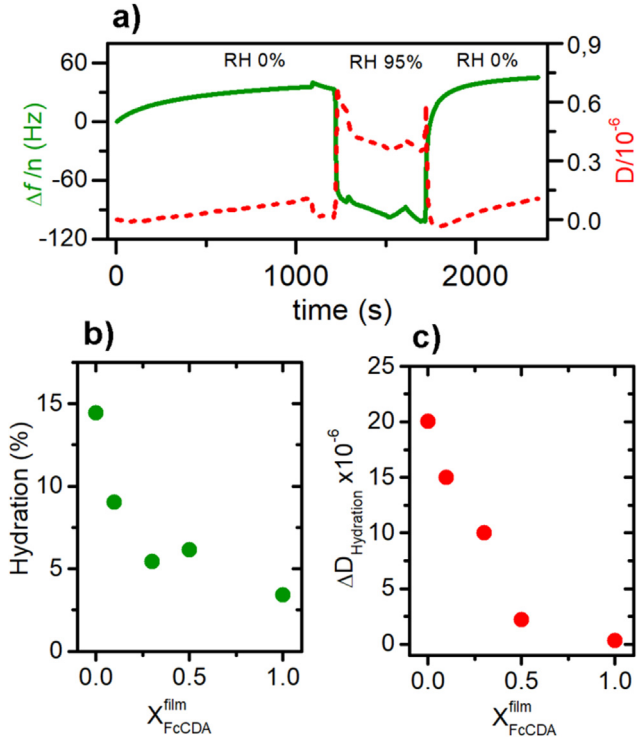

Fig. 2. a) Frequency change (solid line) and dissipation (dashed line) during hydration of $(PAA/FcCDA)_7$. b) Percentage of mass hydration and c) change of dissipation (ΔD) after hydrating the films with different CTA:FcCDA ratios. For these measurements, assemblies of 7 deposition cycles were dehydrated with dry nitrogen (0% RH) and then exposed to a nitrogen atmosphere with a high content of water (95% RH).

the degree of hydration and the dissipation change (Fig. 2a and b) were dependent on the proportion of mixed surfactants in the assembly, results consistent with those obtained from the viscoelastic properties (Fig. 1, bottom).

As the films are very rigid with a low hydration degree and their viscoelastic properties did not show a significant dependence with the nature of the last layer, the mass of PAA (Γ_{PAA}) and surfactants (Γ_{surf}) can be obtained after extracting the water component at the total frequency changes measured by QCM- D.

As it was previously established, the CTA:FcCDA ratio in the films is practically the same as in solution [33], the mole fraction of PAA monomers (X^{film}_{CTA}) and the mole fraction of surfactant (X^{film}_{surf}) in the films is obtained using the monomer molecular weights of PAA (M_w PAA = 72 g/mol) and the molecular weight of CTA and FcCDA, previously given. The apparent molecular weight of the mixed surfactants is given by:

$$M_{surfmixt} = X^{sc}_{CTA} * 284\frac{g}{mol} + X^{sc}_{FcCDA} * 470\frac{g}{mol}$$

where X^{sc}_{CTA} and X^{sc}_{FcCDA} are the molar fraction of the different surfactants in the solution (X^{sc}_{CTA} + X^{sc}_{FcCDA} = 1).

Table 1 presents the surface coverage values of PAA and surfactant obtained for each assembly system after 7 cycles of adsorption. As the CTA fraction for the film preparation decreases, also the PAA fraction in the film (X^{film}_{PAA}) decreases. From the comparison of these results with the hydration study (Fig. 2), it is evident that the degree of hydration of the assemblies increases with the polyacrylate fraction. This last observation was to be expected given that the PAA has a greater polar nature (and therefore higher affinity for water) than the surfactants used with aliphatic chains of 16 carbons long. The C^{film}_{FcCDA} values were obtained as described in the experimental section.

3.2. Electrochemical response

The electron transport throughout the multilayer assemblies prepared from different CTA:FcCDA ratios were studied by cyclic voltammetry (CV). This is a fast and simple technique through which kinetics and mass transport features can be assessed using the shape of the voltammogram and the characteristic peak current and peak potential (i_p and E_p). Studies performed by CV showed that the $(PAA/FcCDA)_5/PAA$ assembly dissolves during the oxidation process, evidenced as a decrease of the faradaic current as a function of the number of cycles. Similar behaviors were previously reported for assemblies of polyanions and polycations that contain a redox center in each monomeric unit [65,66]. The lack of structural stability after the electrochemical oxidation is because a high density of positive charges is produced due to the high concentration of redox centers, causing desorption by electrostatic repulsions [66,67]. Therefore, different mixtures of redox (FcCDA) and non-redox (CTA) surfactants were tested as an approach to decrease the redox centers concentration in the film and, thus, enhance the structural stability. We observed that assemblies prepared from CTA-FcCDA mixtures of $X^{sc}_{FcCDA} \leq 0.5$ displayed good structural stability against oxidation, since the faradaic current and the voltammogram shape remained without significant variations after the 20th CV cycle. Specially, the one with X^{sc}_{FcCDA} = 0.1 undergoes 30 cycles without noticeable changes (Fig. 3a). On the other hand, the peak current as the function of

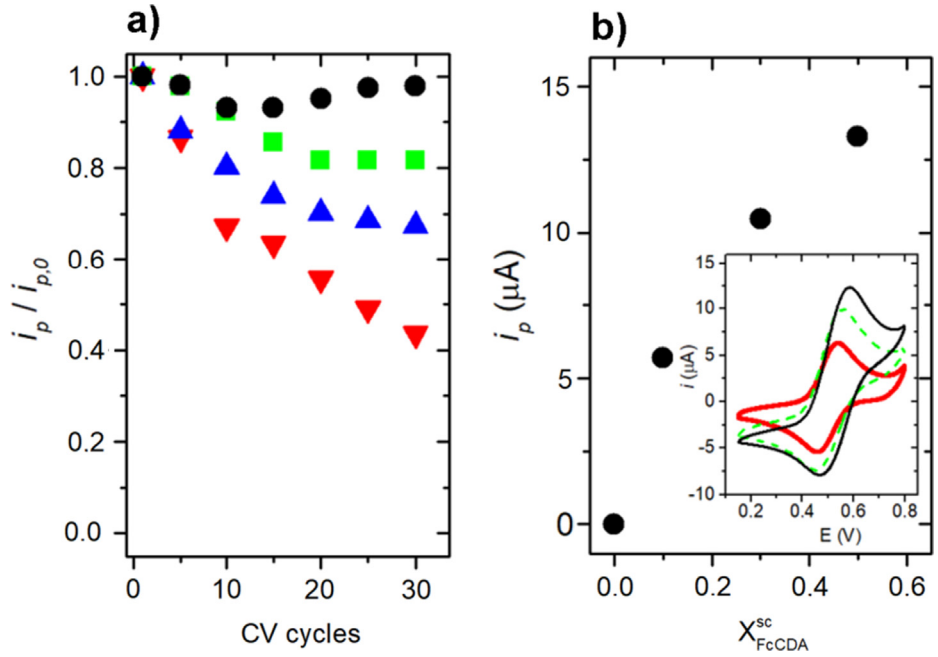

Fig. 3. a) Normalized peak current as a function of the CV cycles for (PAA/surfactants)$_5$/PAA assemblies prepared from X^{sc}_{FcCDA} = 0.1 (●), 0.3 (■), 0.5 (▲), and 1 (▼). b) Peak current as a function of X^{sc}_{FcCDA}, obtained from voltammograms at 10 mV/s. Electrolyte solution: 100 mM KCl. Inset: Cyclic voltammetry response for (PAA/surfactants)$_5$/PAA assemblies (υ = 10 mV/s). X^{sc}_{FcCDA} = 0.1 (red, thick solid line), 0.3 (green, dashed line), and 0.5 (black, thin solid line). (For interpretation of the references to colour in this figure legend, the reader is referred to the web version of this article.)

X^{sc}_{FcCDA} (Fig. 3b) was obtained from their voltammograms (inset), and, as expected, the increase of X^{sc}_{FcCDA} leads to an increase in the faradaic current.

From the results obtained with the quartz microbalance and considering that the ratio between surfactant with and without ferrocene in the film is practically the same as the solution that originates it [33], the number of moles of FcCDA after 5 layers can be established (Table S1). It was obtained that between the systems containing 0.1 and 0.5 redox surfactant fractions, there is a practically 8-fold increase in redox centers, this is due to the increasing amount of mass adsorbed when the FcCDA fraction increases. Observing the voltammogram in Fig. 3 (right, inset), the current relationship between the systems containing 0.1 redox surfactant fraction (red thick line) and the one containing 0.5 (black thin line) is less than the double. On the other hand, the difference between peak current potentials (ΔE_p) is smaller in the system containing fewer ferrocene centers. At first glance, these observations are striking since it is expected that by having a higher number of redox centers, the system will present a better charge transport. Also, the voltammograms show a shift toward higher potential values (i.e., an increase of the formal potential) as the concentration of FcCDA in the films increases. Since the concentrations of redox centers are higher than 100 mM in all cases, the generation of positive charges during oxidation can cause a substantial effect on the formal potential (E^0) of the couple. This parameter has been taken into account since the early papers devoted to the electrochemical response of adsorbed species until our days [68–73]. However, in most of these works, reversible processes are considered that is not the case here where the ΔE_p value reflects a quasireversible process.

The relationship between peak current as a function of the scan rate at different stages of the assembly process is presented in Fig. 4. The values are represented in the logarithmic form since, in this way, the corresponding electrochemical behavior can be assigned depending on the slope value. A slope of 1 corresponds to a thin layer behavior, while a slope of 0.5 corresponds to a

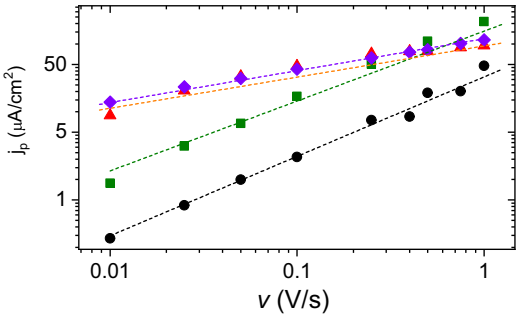

Fig. 4. Peak current density as function of the scan rate at different stages of the layer-by-layer assembly process, n = 1(●), 3(■), 5(▲) and 7(◆) for (PAA/CTA$_{0.9}$-FcCDA$_{0.1}$)$_n$/PAA films. The linear fitting of the data (dashed lines) gives the following slope values: 1.17 (R^2 = 0.990), 1.03 (R^2 = 0.998), 0.49 (R^2 = 0.940) and 0.49 (R^2 = 0.998) for n = 1, 3, 5 and 7 respectively. Experimental conditions: 100 mM KCl.

semi-infinite diffusion-controlled process. It is apparent that for assemblies constituted with 1 and 3 bilayers, the behavior corresponds to a thin layer for almost all the scan rates, while for 5 and 7 bilayers corresponds to a diffusion-controlled process for practically all the scan rates. For example, for 5 bilayers, the maximum scan rate where the voltammogram has a bell shape is at 10 mV s^{-1}, while for 3 bilayers still at 250 mV s^{-1} a distinct bell shape is observed (Fig. S1. Electronic Supplementary material). This sharp change in the charge transport is in accordance with how the film grows from 13 to 40 nm in thickness between 3 and 5 bilayers.

The charge transport through electroactive films involves electron hopping from one reduced molecule to an adjacent oxidized molecule in fixed sites, generating concentration gradients of oxidized and reduced sites, and the flux of counterions to compensate the generated charge within the film. The ingress or egress of ions is a diffusive process presenting a diffusion coefficient that can be

different from the one in solution. The electron hopping process can be described considering the electron as a species that diffuse through the film following Fick's laws [74,75]. In this way, an apparent diffusion coefficient (D_{ap}) is established for electroactive films, which characterizes the ability of the film to propagate the redox process, and is determined by the slowest charge transport mechanism (electron hopping vs. counterion diffusion) [48,61].

The information provided by the cyclic voltammetry experiments at different scan rates was used to feed a numerical model using a finite-element software in which the redox centers are assumed to be confined within the film to obtain kinetics parameters related to the heterogeneous electron transfer rate between the electrode surface and the redox centers (k_0), and the apparent diffusion coefficient (D_{ap}). To simulate the cyclic voltammograms, it is necessary to know the concentration of ferrocene moieties and the thickness of the film. For this purpose, the value of concentration presented in Table 1, the charge from cyclic voltammetries at low scan rates, and the electrode geometrical area were used to calculate the thickness of the film. Taking these two parameters into account and considering the electrode area, the nominal thickness yields a value of 57 nm. D_{ap} and k_0 are determined from the adjustment of the model to experimental cyclic voltammograms to reproduce peak high and peak separation at different scan rates. Fig. 5a and 5b show the fitting for the peak current density and peak potential difference at different scan rates for (PAA/$CTA_{0.9}$-$FcCDA_{0.1}$)$_5$/PAA assembly. These values correspond to simulations carried out taking $D_{ap} = 4 \times 10^{-12}$ cm^2 s^{-1} and $k_0 = 7.5 \times 10^{-7}$ cm s^{-1}.

In Fig. 5c, the experimental voltammogram at a low scan rate (10 mV s^{-1}, thin layer behavior) is represented together with the simulated one. The difference in the shape of the peak can be explained due to the limitation of our simulation model. In the model the interaction between redox centers is not taken into account; therefore, its shape corresponds to an ideally adsorbed species with a quasireversible behavior; while in the experimental voltammograms the repulsion between the charged redox centers generates a broaden peak that can be explained considering that each redox centers present a formal potential depending on its environment [68–73]. A simple representation of this phenomenon is considering the system as a mixture of several species with different formal potential and each of them at a given concentration. Fig. 5d shows the shape for a simulated voltammogram (green thin line) considering 4 species with slight differences in formal potentials and a convenient concentration ratio (see details in the caption figure). In this way, the fitting with the experimental data is improved, supporting the idea of formal potentials dependent on the environment.

D_{ap} values for redox polyelectrolyte-based films go from 10^{-8} to 10^{-13} cm^2 s^{-1}, and it has been demonstrated that the molecular architecture of these systems has an important effect on the resulting charge transport. On the side of highest diffusion values, Heller and coworkers demonstrated that D_{ap} increases with the degree of hydration of the electroactive film, and for highly hydrated films of hydrogels modified with osmium complexes, they reported D_{ap} values close to 10^{-8} cm^2 s^{-1} [76,77]. Regarding layer-by-layer systems, Zambelli and collaborators have reported D_{ap} of 2.50×10^{-10} cm^2 s^{-1} for assemblies of ferrocene-modified polyallylamine (PAH-Fc) and polyglutamic acid (PGA), and D_{ap} of 5.6×10^{-12} cm^2 s^{-1} for assemblies of PAH-Fc and polystyrenesulfonate (PSS) [78]. These authors concluded that a higher value of D_{ap} is showed for polymers layers with grater interdiffusion yielding an increase of the short-range movement of the redox centers and, thus, improving the electron transport. Another interesting example is the work of Tong and collaborators of mesostructured and electroactive films prepared from ionic self-assembly of PSS and redox surfactants of different lengths of the alkyl chain [47]. These authors reported that D_{ap} increases from 1.25×10^{-12} to 17.9×10^{-12} cm^2 s^{-1} as the length of the alkyl chain increases from 7 to 16 carbon atoms. The authors explain this behavior considering that the diffusion of counterions and the charge transport into the film are faster in the derivatives with longer chains due to the more ordered mesomorphous structure formed by the longer surfactant which would supply better channels for electrolyte diffusion and charge transfer. In this work ($D_{ap} = 4 \times 10^{-12}$ cm^2 s^{-1}), the assemblies show well-defined mesostructure, marked hydrophobic character, and high rigidity. Therefore, the ingress of counterions to compensate the charge generated by oxidizing the ferrocene centers is more difficult than the case of highly hydrated hydrogels [76,77], being more similar to the assemblies reported by Tong [47].

3.3. Mass transport

Another aspect to consider in the whole process is the diffusion of the counterions to maintain the electroneutrality inside the film (schematized in Fig. 6a). It has been frequently reported that the flow of electrons occurring in the oxidation process requires the ingress of anions from the solution or the egress of cations present in the film to maintain the condition of electroneutrality [57,79–83]. Also, the flow of ions to compensate for the charge generated is accompanied by the flow of the solvent. In this section, we present the study of the flow of ions and solvent carried out by the quartz crystal microbalance technique with an electrochemical module (EQCM-D) for assemblies (PAA/surfactant)$_n$. The current density (j) and the frequency (Δf) obtained during a cyclic voltammetry experiment using an assembly of (PAA/$CTA_{0.5}$-$FcCDA_{0.5}$)$_7$/PAA and (PAA/$CTA_{0.9}$-$FcCDA_{0.1}$)$_7$/PAA are shown in Figs. 6b and S2 in ESI, respectively. The results show that, as the redox centers of the film are oxidized, an increase in mass occurs (visualized as a decrease of Δf) due to the ingress of anions to maintain the electroneutrality. Once the half cycle is finished, the reverse potential scan is applied to produce the reduction of the redox centers and egress of the counterions. During the experiment, a slight hysteresis was observed in the oxidation/reduction process concerning the mass exchange, an effect already reported [57,84].

The comparison of the changes in frequency (Δf), dissipation (ΔD) and faradaic charge (Q) as a function of time (Fig. 6c) show that the decrease in frequency during the oxidation of the film is accompanied by an slight increase in dissipation. The fact that the changes of Δf and ΔD as a function of Q are practically identical for all harmonics (see curves for n = 3, 5, and 7) is another evidence of the high film rigidity supporting the use of the Sauerbrey equation as a good approximation [82].

Fig. 7 shows the change of Δf and ΔD as a function of the faradic charge during the cyclic voltammetry experiments using sodium salts with anions of different radius: $NO_3^- < Cl^- < SO_4^{2-}$ (see Table 2). These anions represent a benchmark for the study of mass and charge transport in layer-by-layer systems [57,65,85], phenomena that are frequently correlated with the Hofmeister series (and, therefore, with the solvation energy). As is well known, the nature of the anion can have a strong influence on the final properties of charged supramolecular and macromolecular systems [86–88]. Anions that form strong ion pairs with our charged supramolecular assemblies, such as ClO_4^-, were not used to avoid conformation changes and the disassembly of the films [66,89–91]. The chosen anions follow the order $NO_3^- < Cl^- < SO_4^{-2}$ in the Hofmeister series. On the left side of the series, ions are chaotropic, exhibiting weaker interactions with water. On the right side, ions are kosmotropic, exhibiting strong water solvation.

Qualitatively, the results obtained using $NaNO_3$ were similar to those obtained with NaCl. Δf decrease and an slight ΔD increase were observed as the film was oxidized, and the opposite behavior

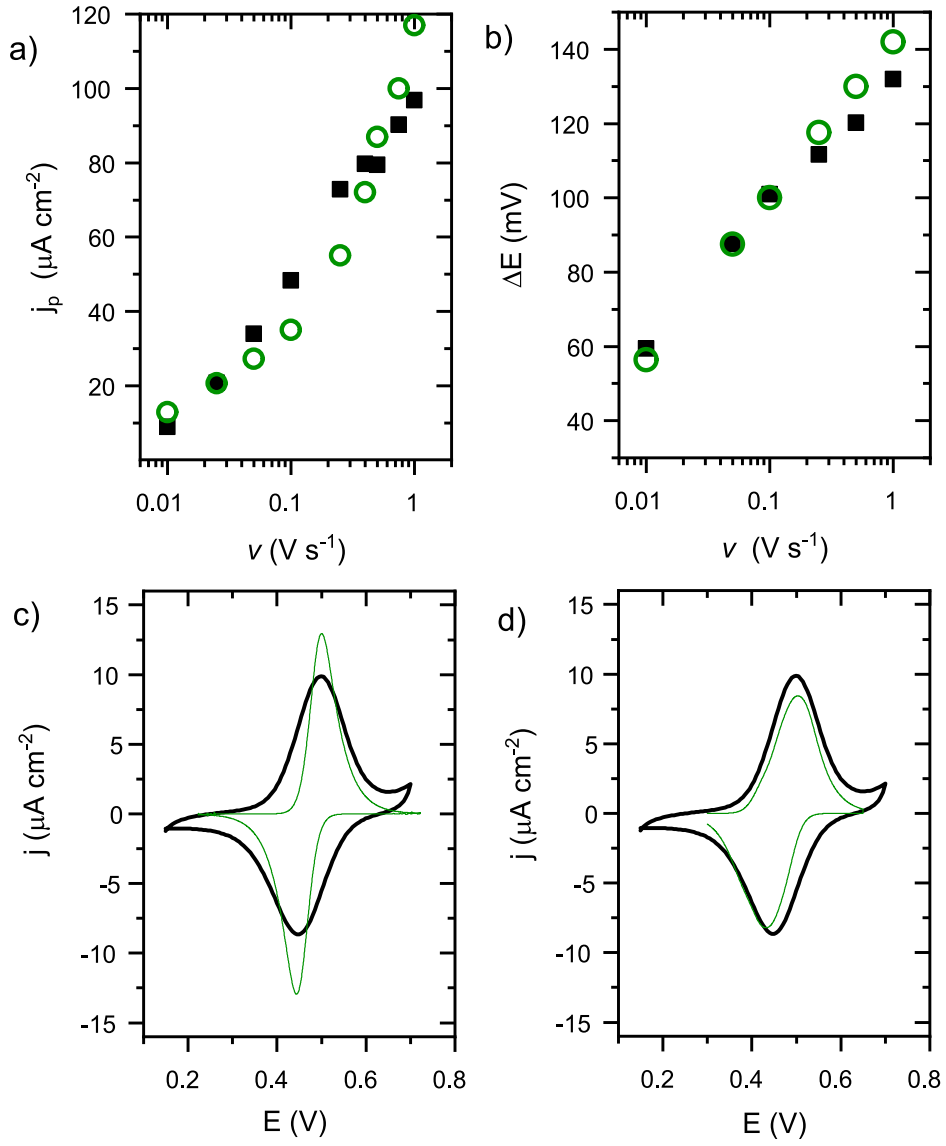

Fig. 5. Peak current density (a) and peak potential (b) versus scan rate for the experimental data (black squares) of the assembly (PAA/$CTA_{0.9}$-$FcCDA_{0.1}$)$_5$/PAA and the simulated data (green circles) assuming $E^{o'}$ = 80.47 V. (c) experimental (black thick lines) and simulated (green thin lines) cyclic voltammograms considering the formal potential is equal to 0.47 V; (d) the simulated voltammogram is the addition of the voltammograms of 4 species with formal potentials equal to 0.40, 0.44, 0.47 and 0.50 V with the following molar fractions: 0.27, 0.27, 0.32 and 0.14, respectively. $D_{ap} = 4 \times 10^{-12}$ cm^2 s^{-1}, $k_0 = 7.5 \times 10^{-7}$ cm s^{-1} and a film thickness of 57 nm was considered for all the simulations. (For interpretation of the references to colour in this figure legend, the reader is referred to the web version of this article.)

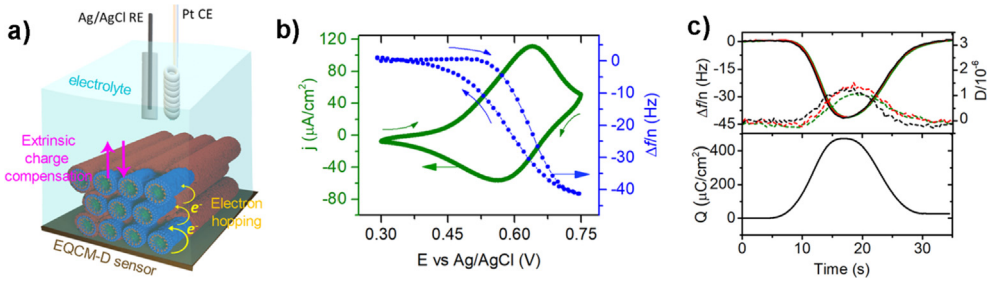

Fig. 6. EQCM-D response for a (PAA/$CTA_{0.5}$-$FcCDA_{0.5}$)$_7$/PAA assembly. a) Scheme of the experimental setup. b) Current density (j) and Δf as a function of the applied potential. c) Frequency change (solid lines), dissipation (dashed lines) and faradaic charge (Q) as function of the time. Frequency and dissipation correspond to the harmonics 3 (green), 5 (red) and 7 (black). All the experiments were carried out in a 100 mM NaCl at a scan rate of 25 mV/s. (For interpretation of the references to colour in this figure legend, the reader is referred to the web version of this article.)

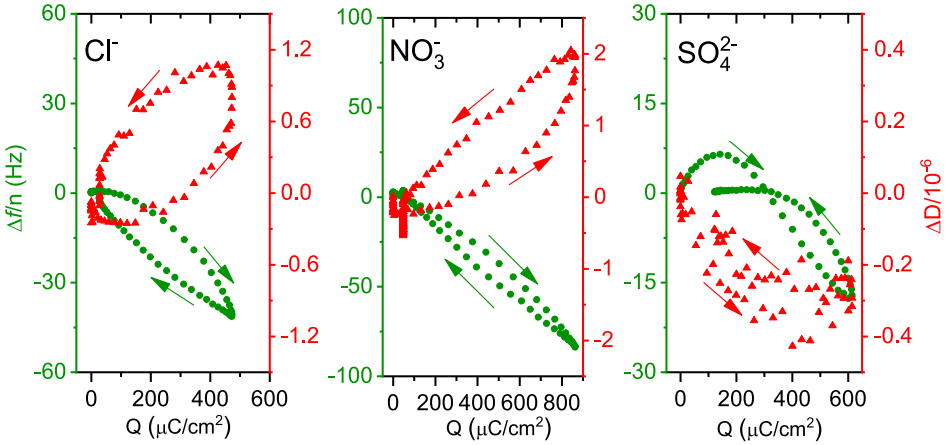

Fig. 7. Δf (green circles) and ΔD (red triangles) as a function of the faradaic charge (Q) for $(PAA/CTA_{0.5}\text{-}FcCDA_{0.5})_7/PAA$. The studies were carried out in NaCl, $NaNO_3$ y Na_2SO_4 solutions at a concentration of 100 mM. Scan rate: 25 mV/s. (For interpretation of the references to colour in this figure legend, the reader is referred to the web version of this article.)

Table 2
Mass to charge relationships and hydration number (N_{H2O}) estimated from EQCM-D data in the presence of different anions.

Anion	$(\Delta m/\Delta Q)^*$/g C^{-1} ($\times 10^3$)	Δm^*/g mol^{-1}	N_{H2O} by EQCM-D	Ionic radius/nm**	N_{H2O} coordination**
NO^{3-}	1.64 ± 0.03	158 ± 2	5.3	0.177	6
Cl^-	1.52 ± 0.18	146 ± 17	6.2	0.180	6–8
$SO4^{2-}$	0.95 ± 0.04	183 ± 8	4.8	0.242	6.4–9.6

* Values are the average and their standard deviations calculated from four different sets of EQCM-D voltammetric experiments measured at 25 mV/s.
** Values reported in Ref. [93].

in the reduction process. On the other hand, the experiments carried out using Na_2SO_4 showed an increase of Δf during the beginning of the oxidation and then a decrease of Δf in the rest of the oxidation process. The observed behavior suggests that in the presence of the SO_4^{2-} anion, the system responds to oxidation by first expelling cations and then capturing anions. The behavior of SO_4^{2-} can be explained by a combination of factors, on the one hand, its stronger interaction with water, and on the other, as it is a divalent ion, the existence of a greater electrostatic repulsion between this ion and the outer layer of PAA of the film (also negative). Similar observations were reported for modified polyallylamine assemblies with osmium complexes (PAH-Os) and polystyrenesulfonate (PSS) [92].

By using the Sauerbrey equation, the mass per unit of charge was obtained that allows estimating the number of water molecules that accompany the entry of each anion. Table 2 compiles the values of mass exchanged per unit of charge ($\Delta m/\Delta Q$), the molar mass exchanged (Δm), and the number of water molecules (N_{H2O}) for each anion as the film goes from the reduced to the oxidized state. It is interesting to note that N_{H2O} values are equal to, or less than, the hydration sphere of the anion in solution. This observation differs from that obtained for multilayer assemblies of modified polyallylamine with complexes of osmium (PAH-Os) and polystyrenesulfonate (PSS) [92] and for assemblies of PAH-Os and glucose oxidase (GOx) [94] where the entry of anion is accompanied by a large number of water molecules (N_{H2O} ranging from 15 to 30). Tagliazucchi et al. simulated the ingress of the solvent employing a molecular theory [95] and suggested a simplified mechanical description of this phenomenon: "on the one hand, the osmotic pressure of the ions and the electrostatic forces tend to swell the film to reduce the differences in electrolyte concentration inside and outside the film and to minimize the repulsion between the charged species. On the other, the elasticity of the polymer (conformational entropy), the hydrophobic interactions between segments, and the attraction between positive/negative macromolecules counteract these forces, preventing the thickness from increasing indefinitely (i.e., the film completely desorbs). The thickness reaches equilibrium when the balance of these effects becomes zero" [96]. Therefore, the particularities found in our systems in terms of the amount of water entering per counterion are possibly due to the strong polyanion/cationic-surfactant (ion pairs) and surfactant-surfactant (hydrophobic) interactions resulting in very compact assemblies with a high degree of order that limits the entry of water.

Although the flow of Cl^- and NO_3^- anions come along with a quantity of water (N_{H2O}) corresponding to its hydration sphere, in the case of SO_4^{2-} this value was somewhat lower. Failure to obtain an increase in dissipation during oxidation in the presence of SO_4^{2-} is consistent with the low amount of water ingress. Since the sulfate is the largest anion, the observed behavior could be due to the fact that the assemblies are so compact and ordered that they could limit the entry of water molecules for this bulky anion.

3.4. Anion effect on the charge transport

The charge transport through the electroactive films was studied in electrolytes containing anions with different radius: NO_3^- < Cl^- < SO_4^{2-}. Voltammograms were carried out at different scan rates (Fig. 8). It can be appreciated that the nature of the anion had a significant impact on the electrochemical properties of the films. The efficiency of the charge transport is NO_3^- > Cl^- > SO_4^{2-}. Therefore, the results indicate that the size of the anion plays an essential role in the electrochemical response of these highly organized and compact electroactive films. A detailed study with more salts should be carried out to corroborate this hypothesis.

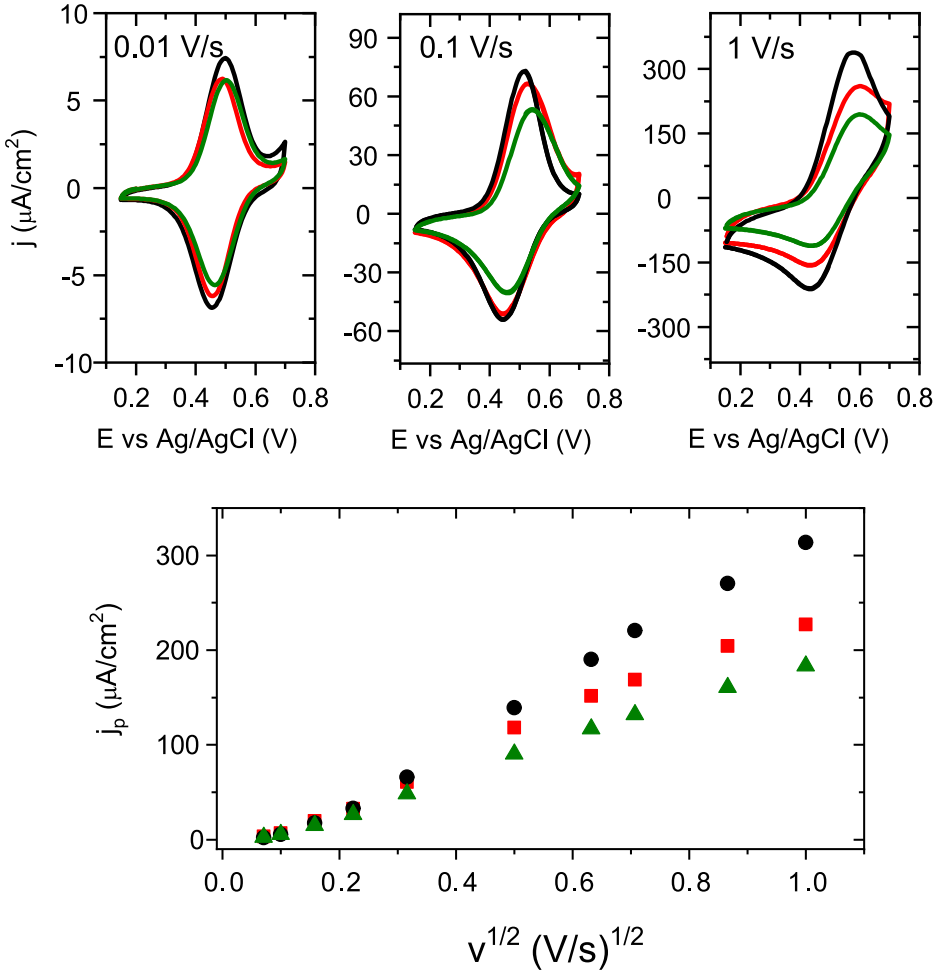

Fig. 8. Cyclic voltammograms (top) and peak current density as a function of the square root of the scan rate (bottom) for a (PAA/$CTA_{0.5}$-$FcCDA_{0.5}$)$_5$/PAA film. The electrochemical experiments were carried out in different electrolytes: 100 mM $NaNO_3$ (black circles), 100 mM NaCl (red squares), 100 mM Na_2SO_4 (green triangles). (For interpretation of the references to colour in this figure legend, the reader is referred to the web version of this article.)

4. Conclusions

We demonstrated in this work that the layer-by-layer assembly of polyelectrolytes and different mixtures of redox and non-redox surfactants allows the generation of a rigid structure with a low content of water presenting a quasireversible electrochemical response. This behavior represents an exciting feature since the system can carry out an efficient electron transport through the film preserving its structure (dissipation changes are negligible).

In previous works devoted to electron transfer in layer-by-layer hydrogels, significant changes (up to 20%) in the water content of the film were observed [79,81–84,97]. As these materials present a viscoelastic behavior, the successive cycles of the electrochemical treatment leads to changes in their structures, as it was demonstrated by Sun et al. [98], where the hydrogeĺs thickness and Youngś modulus change at each cycle. On the other hand, our approach is complementary to previous works related to polyelectrolyte-surfactant systems where the redox moiety is grafted on the polyelectrolyte, and the studies are centered in the *meso*-structure obtained by changing the surfactants [37,99,100]. Here, we have used the ordered *meso*-structure to build a stable electroactive interface. Finally, ferrocenyl surfactants have been a matter of research for several years; however, these studies were mainly focused on exploiting the changes in aggregate microstructures, surface tension, and redox properties that can be achieved by manipulating in the oxidation states [101–106].

The precise control over the *meso*-organization and the stability through the redox process presented by these assemblies makes them promising components in the construction of devices where the vectorial transfer of electrons, or ions, is required. For example, by oxidation of the ferrocenyl moiety, the film can be loaded with a specific anion, which can be released by its reduction. On the other hand, its assembly on transparent electrodes (e.g., ITO) could lead to electrochromic devices since ferrocene in its reduced state is amber (maximum absorbance at 445 nm), while in its oxidized state turns blue (maximum absorbance at 619 nm) [106].

CRediT authorship contribution statement

Esteban Piccinini: Conceptualization, Investigation, Methodology, Formal analysis, Writing - original draft. **Graciela A. González:** Conceptualization, Formal analysis, Writing - original draft. **Omar Azzaroni:** Conceptualization, Formal analysis, Supervision, Writing - review & editing. **Fernando Battaglini:** Conceptualization, Formal analysis, Supervision, Writing - review & editing.

Declaration of Competing Interest

The authors declare that they have no known competing financial interests or personal relationships that could have appeared to influence the work reported in this paper.

Acknowledgements

This work was supported by the following institutions: Universidad de Buenos Aires (UBACYT 20020170100341BA), PIP CONICET (11220150100291CO), Universidad Nacional de La Plata (UNLP) (PPID-X016), ANPCYT, Argentina (PICT 2015-0801, 2016-1680, 2017-1523), and CONICET (PIP-0370). G.A.G., F.B. and O.A. are staff members of CONICET. E.P. acknowledges a postdoctoral fellowship from CONICET.

Appendix A. Supplementary data

Supplementary data to this article can be found online at https://doi.org/10.1016/j.jcis.2020.07.060.

References

[1] H.E. Katz, J. Huang, Thin-film organic electronic devices, Annu. Rev. Mater. Res. 39 (2009) 71–92. ST-Thin-Film Org. Electron. Dev. doi:10.1146/annurev-matsci-082908-145433.
[2] T. Nakanishi, Supramolecular Soft Matter, John Wiley & Sons, Inc., Hoboken, NJ, USA, 2011. doi:10.1002/9781118095331.
[3] C.M. Palumbiny, F. Liu, T.P. Russell, A. Hexemer, C. Wang, P. Müller-Buschbaum, The crystallization of PEDOT:PSS polymeric electrodes probed in situ during printing, Adv. Mater. 27 (2015) 3391–3397, https://doi.org/10.1002/adma.201500315.
[4] J.Y. Park, R.C. Advincula, Nanostructuring polymers, colloids, and nanomaterials at the air–water interface through Langmuir and Langmuir-Blodgett techniques, Soft Matter. 7 (2011) 9829, https://doi.org/10.1039/c1sm05750b.
[5] D.T. Balogh, M. Ferreira, O.N. Oliveria, Langmuir–Blodgett–Kuhn multilayer assemblies: past, present, and future of the LB technology, in: R.C. Advincula, W. Knoll (Eds.), Funct. Polym. Film., Wiley-VCH Verlag & Co. KGaA, Weinheim, Germany, 2011, pp. 113–149.
[6] K. Ariga, Y. Yamauchi, G. Rydzek, Q. Ji, Y. Yonamine, K.-C.-W. Wu, J.P. Hill, Layer-by-layer nanoarchitectonics: invention, innovation, and evolution, Chem. Lett. 43 (2014) 36–68, https://doi.org/10.1246/cl.130987.
[7] J. Wang, J. Tang, B. Ding, V. Malgras, Z. Chang, X. Hao, Y. Wang, H. Dou, X. Zhang, Y. Yamauchi, Hierarchical porous carbons with layer-by-layer motif architectures from confined soft-template self-assembly in layered materials, Nat. Commun. 8 (2017) 1–9, https://doi.org/10.1038/ncomms15717.
[8] V.C. Rodrigues, M.L. Moraes, J.C. Soares, A.C. Soares, R. Sanfelice, E. Deffune, O. N. Oliveira, Immunosensors made with layer-by-layer films on chitosan/gold nanoparticle matrices to detect D-dimer as biomarker for venous thromboembolism, Bull. Chem. Soc. Jpn. 91 (2018) 891–896, https://doi.org/10.1246/bcsj.20180019.
[9] J.M. Elliott, J.R. Owen, Electrochemical impedance characterisation of a nanostructured (mesoporous) platinum film, Phys. Chem. Chem. Phys. 2 (2000) 5653–5659, https://doi.org/10.1039/b006462i.
[10] M.L. Cortez, N. De Matteis, M. Ceolín, W. Knoll, F. Battaglini, O. Azzaroni, Hydrophobic interactions leading to a complex interplay between bioelectrocatalytic properties and multilayer meso-organization in layer-by-layer assemblies, Phys. Chem. Chem. Phys. 16 (2014) 20844–20855, https://doi.org/10.1039/c4cp02334j.
[11] T.S. Metzger, R. Tel-Vered, I. Willner, Controlled vectorial electron transfer and photoelectrochemical applications of layered relay/photosensitizer-imprinted Au nanoparticle architectures on electrodes, Small 12 (2016) 1605–1614, https://doi.org/10.1002/smll.201503077.
[12] M.L. Cortez, A. Lorenzo, W. Marmisollé, C. von Bilderling, E. Maza, L.I. Pietrasanta, F. Battaglini, M. Ceolín, O. Azzaroni, Highly-organized stacked multilayers via layer-by-layer assembly of lipid-like surfactants and polyelectrolytes. Stratified supramolecular structures for (bio)electrochemical nanoarchitectonics, Soft Matter 14 (2018) 1939–1952. doi:10.1039/C8SM00052B.
[13] K. Silambarasan, J. Joseph, Electrochemical diagnosis of chemical switch: impact of structural changes on charge transport mechanism of "redox anion bound polysilsesquioxane" film, ChemElectroChem. 5 (2018) 2808–2815, https://doi.org/10.1002/celc.201800799.
[14] M. Aono, Y. Bando, K. Ariga, Nanoarchitectonics: pioneering a new paradigm for nanotechnology in materials development, Adv. Mater. 24 (2012) 150–151, https://doi.org/10.1002/adma.201104614.
[15] M. Ramanathan, L.K. Shrestha, T. Mori, Q. Ji, J.P. Hill, K. Ariga, Amphiphile nanoarchitectonics: from basic physical chemistry to advanced applications, Phys. Chem. Chem. Phys. 15 (2013) 10580, https://doi.org/10.1039/c3cp50620g.
[16] K. Ariga, M. Ito, T. Mori, S. Watanabe, J. Takeya, Atom/molecular nanoarchitectonics for devices and related applications, Nano Today 28 (2019), https://doi.org/10.1016/j.nantod.2019.07.001 100762.
[17] K. Ariga, X. Jia, J. Song, J.P. Hill, D.T. Leong, Y. Jia, J. Li, Nanoarchitectonics beyond self-assembly: challenges to create bio-like hierarchic organization, Angew. Chem. Int. Ed. (2020), https://doi.org/10.1002/anie.202000802.
[18] R.K. Iler, Multilayers of colloidal particles, J. Colloid Interface Sci. 21 (1966) 569–594, https://doi.org/10.1016/0095-8522(66)90018-3.
[19] G. Decher, J.-D. Hong, Buildup of ultrathin multilayer films by a self-assembly process, I. Consecutive adsorption of anionic and cationic bipolar amphiphiles on charged surfaces, Makromol. Chemie. Macromol. Symp. 46 (1991) 321–327, https://doi.org/10.1002/masy.19910460145.
[20] G. Decher, J.D. Hong, Buildup of ultrathin multilayer films by a self-assembly process: II. Consecutive adsorption of anionic and cationic bipolar amphiphiles and polyelectrolytes on charged surfaces, Ber. Bunsen. Phys. Chem. 95 (1991) 1430–1434. doi:10.1002/bbpc.19910951122.
[21] S. Zhao, F. Caruso, L. Dahne, G. Decher, B.G. De Geest, J. Fan, N. Feliu, Y. Gogotsi, P.T. Hammond, M.C. Hersam, A. Khademhosseini, N. Kotov, S. Leporatti, Y. Li, F. Lisdat, L.M. Liz-Marzan, S. Moya, P. Mulvaney, A.L. Rogach, S. Roy, D.G. Shchukin, A.G. Skirtach, M.M. Stevens, G.B. Sukhorukov, P.S. Weiss, Z. Yue, D. Zhu, W.J. Parak, The future of layer-by-layer assembly: a tribute To ACS Nano associate editor Helmuth Mohwald, ACS Nano 13 (2019) 6151–6169, https://doi.org/10.1021/acsnano.9b03326.
[22] K. Ariga, J.P. Hill, Q. Ji, Layer-by-layer assembly as a versatile bottom-up nanofabrication technique for exploratory research and realistic application, Phys. Chem. Chem. Phys. 9 (2007) 2319–2340, https://doi.org/10.1039/b700410a.
[23] G. Decher, J.B. Schlenoff, Multilayer Thin Films: Sequential Assembly of Nanocomposite Materials, 2nd ed., WILEY-VCH Verlag GmbH & Co, Weinheim, 2012.
[24] R.M. Iost, F.N. Crespilho, Layer-by-layer self-assembly and electrochemistry: Applications in biosensing and bioelectronics, Biosens. Bioelectron. 31 (2012) 1–10, https://doi.org/10.1016/j.bios.2011.10.040.
[25] E. Piccinini, C. Bliem, C. Reiner-Rozman, F. Battaglini, O. Azzaroni, W. Knoll, Enzyme-polyelectrolyte multilayer assemblies on reduced graphene oxide field-effect transistors for biosensing applications, Biosens. Bioelectron. 92 (2017) 661–667, https://doi.org/10.1016/j.bios.2016.10.035.
[26] M. Lösche, J. Schmitt, G. Decher, W.G. Bouwman, K. Kjaer, Detailed structure of molecularly thin polyelectrolyte multilayer films on solid substrates as revealed by neutron reflectometry, Macromolecules 31 (1998) 8893–8906, https://doi.org/10.1021/ma980910p.
[27] D. Korneev, Y. Lvov, G. Decher, J. Schmitt, S. Yaradaikin, Neutron reflectivity analysis of self-assembled film superlattices with alternate layers of deuterated and hydrogenated polysterenesulfonate and polyallylamine, Phys. B. 213–214 (1995) 954–956, https://doi.org/10.1016/0921-4526(95)00333-5.
[28] G.J. Kellogg, A.M. Mayes, W.B. Stockton, M. Ferreira, M.F. Rubner, S.K. Satija, Neutron Reflectivity Investigations of Self-Assembled Conjugated Polyion Multilayers, Langmuir. 12 (1996) 5109–5113. doi:10.1021/la960285m.
[29] D. Yoo, S.S. Shiratori, M.F. Rubner, Controlling bilayer composition and surface wettability of sequentially adsorbed multilayers of weak polyelectrolytes, Glass 9297 (1998) 4309–4318, https://doi.org/10.1021/ma9800360.
[30] X. Arys, P. Fischer, A.M. Jonas, M.M. Koetse, A. Laschewsky, R. Legras, E. Wischerhoff, Ordered polyelectrolyte multilayers. Rules governing layering in organic binary multilayers, J. Am. Chem. Soc. 125 (2003) 1859–1865, https://doi.org/10.1021/ja0283807.
[31] X. Arys, A. Laschewsky, A.M. Jonas, Ordered polyelectrolyte "multilayers" – 1. Mechanisms of growth and structure formation: a comparison with classical fuzzy "multilayers", Macromolecules 34 (2001) 3318–3330, https://doi.org/10.1021/ma010092s.
[32] E. Piccinini, J.S. Tuninetti, J. Irigoyen Otamendi, S.E. Moya, M. Ceolín, F. Battaglini, O. Azzaroni, Surfactants as mesogenic agents in layer-by-layer assembled polyelectrolyte/surfactant multilayers: nanoarchitectured "soft" thin films displaying a tailored mesostructure, Phys. Chem. Chem. Phys. 20 (2018) 9298–9308. doi:10.1039/C7CP08203G.
[33] E. Piccinini, M. Ceolín, M. Battaglini, O. Azzaroni, Mesostructured electroactive thin films through layer-by-layer assembly. nanoarchitectonics and mesoscale organization going hand-in-hand, Chempluschem. in press (2020). doi:10.1002/cplu.202000358.
[34] C.T. Kresge, M.E. Leonowicz, W.J. Roth, J.C. Vartuli, J.S. Beck, Ordered mesoporous molecular sieves synthesized by a liquid-crystal template mechanism, Nature 359 (1992) 710–712, https://doi.org/10.1038/359710a0.
[35] C.J. Brinker, Y. Lu, A. Sellinger, H. Fan, Evaporation-induced self-assembly : nanostructures made easy, Adv. Mater. 11 (1999) 579–585. doi:10.1002/(SICI)1521-4095(199905)11:7<579::AID-ADMA579>3.3.CO;2-I.
[36] A. Walcarius, Mesoporous materials and electrochemistry, Chem. Soc. Rev. 42 (2013) 4098–4140, https://doi.org/10.1039/c2cs35322a.
[37] C.F.J. Faul, Ionic self-assembly for functional hierarchical nanostructured materials, Acc. Chem. Res. 47 (2014) 3428–3438, https://doi.org/10.1021/ar500162a.
[38] M. Antonietti, C. Burger, J. Effing, Mesomorphous polyelectrolyte-surfactant complexes, Adv. Mater. 7 (1995) 751–753, https://doi.org/10.1002/adma.19950070817.
[39] M.L. Cortez, D. Pallarola, M. Ceolín, O. Azzaroni, F. Battaglini, Ionic self-assembly of electroactive biorecognizable units: electrical contacting of redox glycoenzymes made easy, Chem. Commun. 48 (2012) 10868–10870, https://doi.org/10.1039/c2cc35949a.
[40] M.L. Cortez, D. Pallarola, M. Ceolín, O. Azzaroni, F. Battaglini, Electron transfer properties of dual self-assembled architectures based on specific recognition and electrostatic driving forces: Its application to control substrate inhibition in horseradish peroxidase-based sensors, Anal. Chem. 85 (2013) 2414–2422, https://doi.org/10.1021/ac303424t.

[41] M.L. Cortez, M. Ceolín, L.C. Camacho, E. Donath, S.E. Moya, F. Battaglini, O. Azzaroni, Solvent effects on the structure-property relationship of redox-Active self-Assembled nanoparticle-polyelectrolyte-surfactant composite thin films: implications for the generation of bioelectrocatalytic signals in enzyme-containing assemblies, ACS Appl. Mater. Interfaces 9 (2017) 1119–1128, https://doi.org/10.1021/acsami.6b13456.
[42] M.L. Cortez, M. Ceolín, O. Azzaroni, F. Battaglini, Formation of redox-active self-assembled polyelectrolyte-surfactant complexes integrating glucose oxidase on electrodes: Influence of the self-assembly solvent on the signal generation, Bioelectrochemistry 105 (2015), https://doi.org/10.1016/j.bioelechem.2015.06.001.
[43] B.M.D. O'Driscoll, E. Milsom, C. Fernandez-Martin, L. White, S.J. Roser, K.J. Edler, Thin films of polyethylenimine and alkyltrimethylammonium bromides at the air/water interface, Macromolecules 38 (2005) 8785–8794, https://doi.org/10.1021/ma050469k.
[44] K.J. Edler, B. Yang, Formation of mesostructured thin films at the air/water interface, Chem. Soc. Rev. 42 (2013) 3765–3776, https://doi.org/10.1016/j.tsf.2005.08.300.
[45] C. Gustavsson, M. Obiols-Rabasa, L. Piculell, Water-insoluble surface coatings of polyion-surfactant ion complex salts respond to additives in a surrounding aqueous solution, Langmuir 31 (2015) 6487–6496, https://doi.org/10.1021/acs.langmuir.5b00831.
[46] C. Gustavsson, J. Li, K.J. Edler, L. Piculell, Water-responsive internally structured polymer – surfactant films on solid surfaces, Langmuir 30 (2014) 12525–12531, https://doi.org/10.1021/la503210g.
[47] Z. Cheng, B. Ren, M. Gao, X. Liu, Z. Tong, Ionic self-assembled redox-active polyelectrolyte-ferrocenyl surfactant complexes: Mesomorphous structure and electrochemical behavior, Macromolecules 40 (2007) 7638–7643, https://doi.org/10.1021/ma071072e.
[48] M.L. Cortez, G.A. González, M. Ceolín, O. Azzaroni, F. Battaglini, Self-assembled redox polyelectrolyte-surfactant complexes: Nanostructure and electron transfer characteristics of supramolecular films with built-in electroactive chemical functions, Electrochim. Acta 118 (2014) 124–129, https://doi.org/10.1016/j.electacta.2013.11.188.
[49] M.L. Cortez, M. Ceolín, O. Azzaroni, F. Battaglini, Electrochemical sensing platform based on polyelectrolyte-surfactant supramolecular assemblies incorporating carbon nanotubes, Anal. Chem. 83 (2011) 8011–8018, https://doi.org/10.1021/ac202213t.
[50] M.L. Cortez, W. Marmisollé, D. Pallarola, L.I. Pietrasanta, D.H. Murgida, M. Ceolín, O. Azzaroni, F. Battaglini, Effect of gold nanoparticles on the structure and electron-transfer characteristics of glucose oxidase redox polyelectrolyte-surfactant complexes, Chem. – A Eur. J. 20 (2014) 13366–13374, https://doi.org/10.1002/chem.201402707.
[51] M. Yang, Y. Hou, N.A. Kotov, Graphene-based multilayers: Critical evaluation of materials assembly techniques, Nano Today 7 (2012) 430–447, https://doi.org/10.1016/j.nantod.2012.08.006.
[52] J.S. Facci, P.A. Falcigno, J.M. Gold, Characterization of electroactive Langmuir-Blodgett monolayers of (ferrocenylmethyl)dimethyloctadecylammonium sulfate at gold and air/water interfaces, Langmuir 2 (1986) 732–738, https://doi.org/10.1021/la00072a010.
[53] C.A. Goss, C.J. Miller, M. Majda, Microporous aluminum oxide films at electrodes. 5. Mechanism of the lateral charge transport in bilayer assemblies of electroactive amphiphiles, J. Phys. Chem. 92 (1988) 1937–1942, https://doi.org/10.1108/eb019362.
[54] H. Okuda, T. Imae, S. Ikeda, The adsorption of cetyltrimethylammonium bromide on aqueous surfaces of sodium bromide solutions, Colloids Surf. 27 (1987) 187–200, https://doi.org/10.1016/0166-6622(87)80142-7.
[55] K. Patel, O.Š. Miljanić, J.F. Stoddart, Iodide-catalysed self-assembly of donor–acceptor [3]catenanes, Chem. Commun. 51 (2008) 1853–1855, https://doi.org/10.1039/B716245F.
[56] K.A. Marx, Quartz crystal microbalance: a useful tool for studying thin polymer films and complex biomolecular systems at the solution – Surface interface, Biomacromolecules 4 (2003) 1099–1120, https://doi.org/10.1021/bm020116i.
[57] M. Tagliazucchi, D. Grumelli, E.J. Calvo, Nanostructured modified electrodes: role of ions and solvent flux in redox active polyelectrolyte multilayer films, Phys. Chem. Chem. Phys. 8 (2006) 5086–5095, https://doi.org/10.1039/b609341h.
[58] J. Yánez-Heras, G.A. Planes, F. Williams, C.A. Barbero, F. Battaglini, Sequential electrochemical polymerization of aniline and their derivatives showing electrochemical activity at neutral pH, Electroanalysis 22 (2010) 2801–2808, https://doi.org/10.1002/elan.201000325.
[59] J.L. Antonio, L. Höfler, T. Lindfors, S.I. Córdoba de Torresi, Electrocontrolled swelling and water uptake of a three-dimensional conducting polypyrrole hydrogel, ChemElectroChem 3 (2016) 2146–2152, https://doi.org/10.1002/celc.201600397.
[60] W. Kutner, K. Doblhofer, Simultaneous cyclic voltammetry and electrochemical quartz-crystal microbalance study at polymer film-modified electrodes of molecular inclusion of ferrocene by β-cyclodextrin polymer and carboxymethylated β-cyclodextrin polymer as well as ferrocenecarbox, J. Electroanal. Chem. 326 (1992) 139–160, https://doi.org/10.1016/0022-0728(92)80509-3.
[61] V. Flexer, K.F.E. Pratt, F. Garay, P.N. Bartlett, E.J. Calvo, Relaxation and Simplex mathematical algorithms applied to the study of steady-state electrochemical responses of immobilized enzyme biosensors: comparison with experiments, J. Electroanal. Chem. 616 (2008) 87–98, https://doi.org/10.1016/J.JELECHEM.2008.01.006.
[62] J.J. Iturri Ramos, S. Stahl, R.P. Richter, S.E. Moya, Water content and buildup of poly(diallyldimethylammonium chloride)/poly(sodium 4-styrenesulfonate) and poly(allylamine hydrochloride)/poly(sodium 4-styrenesulfonate) polyelectrolyte multilayers studied by an in situ combination of a quartz crystal microb, Macromolecules 43 (2010) 9063–9070, https://doi.org/10.1021/ma1015984.
[63] D. Johannsmann, The Quartz Crystal Microbalance in Soft Matter Research, Springer International Publishing (2015), https://doi.org/10.1007/978-3-319-07836-6.
[64] M. Schönhoff, V. Ball, A.R. Bausch, C. Dejugnat, N. Delorme, K. Glinel, R. v. Klitzing, R. Steitz, Hydration and internal properties of polyelectrolyte multilayers, Colloids Surf. A 303 (2007) 14–29. doi:10.1016/j.colsurfa.2007.02.054.
[65] J. Song, D. Jańczewski, Y. Ma, L. Van Ingen, C. Ee Sim, Q. Goh, J. Xu, G.J. Vancso, Electrochemically controlled release of molecular guests from redox responsive polymeric multilayers and devices, Eur. Polym. J. 49 (2013) 2477–2484, https://doi.org/10.1016/j.eurpolymj.2013.01.029.
[66] J. Song, D. Jańczewski, Y. Ma, M. Hempenius, J. Xu, G.J. Vancso, Disassembly of redox responsive poly(ferrocenylsilane) multilayers: the effect of blocking layers, supporting electrolyte and polyion molar mass, J. Colloid Interface Sci. 405 (2013) 256–261, https://doi.org/10.1016/j.jcis.2013.05.008.
[67] Y. Ma, W.-F. Dong, M.A. Hempenius, H. Möhwald, G.J. Vancso, Redox-controlled molecular permeability of composite-wall microcapsules, Nat. Mater. 5 (2006) 724–729, https://doi.org/10.1038/nmat1716.
[68] E. Laviron, Surface linear potential sweep voltammetry. Equation of the peaks for a reversible reaction when interactions between the adsorbed molecules are taken into account, J. Electroanal. Chem. 52 (1974) 395–402, https://doi.org/10.1016/S0022-0728(74)80449-3.
[69] A.P. Brown, F.C. Anson, Cyclic and Differential pulse voltammetric behavior of reactants confined to the electrode surface, Anal. Chem. 49 (1977) 1589–1595, https://doi.org/10.1021/ac50019a033.
[70] E. Laviron, The use of linear potential sweep voltammetry and of a.c. voltammetry for the study of the surface electrochemical reaction of strongly adsorbed systems and of redox modified electrodes, J. Electroanal. Chem. 100 (1979) 263–270, https://doi.org/10.1016/S0022-0728(79)80167-9.
[71] M. Tagliazucchi, E.J. Calvo, I. Szleifer, A molecular theory of chemically modified electrodes with self-assembled redox polyelectrolyte thin films: Reversible cyclic voltammetry, Electrochim. Acta 53 (2008) 6740–6752, https://doi.org/10.1016/j.electacta.2008.01.041.
[72] M. Tagliazucchi, E.J. Calvo, Charge transport in redox polyelectrolyte multilayer films: the dramatic effects of outmost layer and solution ionic strength, ChemPhysChem. 11 (2010) 2957–2968, https://doi.org/10.1002/cphc.201000172.
[73] O. Alévêque, E. Levillain, A generalized lateral interactions function to fit voltammetric peaks of self-assembled monolayers, Electrochem. Commun. 67 (2016) 73–79, https://doi.org/10.1016/j.elecom.2016.04.003.
[74] D.N. Blauch, J.M. Savéant, Dynamics of electron hopping in assemblies of redox centers. Percolation and diffusion, J. Am. Chem. Soc. 114 (1992) 3323–3332, https://doi.org/10.1021/ja00035a025.
[75] E.F. Dalton, N.A. Surridge, J.C. Jernigan, K.O. Wilbourn, J.S. Facci, R.W. Murray, Charge transport in electroactive polymers consisting of fixed molecular redox sites, Chem. Phys. 141 (1990) 143–157, https://doi.org/10.1016/0301-0104(90)80026-T.
[76] A. Aoki, A. Heller, Electron diffusion coefficients in hydrogels formed of cross-linked redox polymers, J. Phys. Chem. 97 (1993) 11014–11019, https://doi.org/10.1021/j100144a019.
[77] T.J. Ohara, R. Rajagopalan, A. Heller, Glucose electrodes based on cross-linked [Os(bpy)2Cl]+/2+ complexed poly(1-vinylimidazole) films, Anal. Chem. 65 (1993) 3512–3517, https://doi.org/10.1021/ac00071a031.
[78] R. Zahn, G. Coullerez, J. Vörös, T. Zambelli, Effect of polyelectrolyte interdiffusion on electron transport in redox-active polyelectrolyte multilayers, J. Mater. Chem. 22 (2012) 11073, https://doi.org/10.1039/c2jm30469d.
[79] D.J. Schmidt, F.Ç. Cebeci, Z.I. Kalcioglu, S.G. Wyman, C. Ortiz, K.J. Van Vliet, P.T. Hammond, Electrochemically controlled swelling and mechanical properties of a polymer nanocomposite, ACS Nano 3 (2009) 2207–2216, https://doi.org/10.1021/nn900526c.
[80] M. Tagliazucchi, D. Grumelli, C. Bonazzola, E.J. Calvo, Oxidation-reduction dynamics in layer-by-layer self-assembled redox polyelectrolyte multilayer modified electrodes, J. Nanosci. Nanotechnol. 6 (2006) 1731–1740, https://doi.org/10.1166/jnn.2006.237.
[81] D.E. Grumelli, F. Garay, C.A. Barbero, E.J. Calvo, Dynamics of ion exchange between self-assembled redox polyelectrolyte multilayer modified electrode and liquid electrolyte, J. Phys. Chem. B 110 (2006) 15345–15352, https://doi.org/10.1021/jp062282g.
[82] R. Zahn, F. Boulmedais, J. Vörös, P. Schaaf, T. Zambelli, Ion and solvent exchange processes in PGA/PAH polyelectrolyte multilayers containing ferrocyanide, J. Phys. Chem. B 114 (2010) 3759–3768, https://doi.org/10.1021/jp9106074.
[83] I. Jureviciute, S. Bruckenstein, A. Robert Hillman, A. Jackson, Kinetics of redox switching of electroactive polymers using the electrochemical quartz crystal microbalance. Part I. Identifying the rate limiting step in the presence of coupled electron/ion and solvent transfer, Phys. Chem. Chem. Phys. 2 (2000) 4193–4198, https://doi.org/10.1039/b003703f.
[84] I. Jureviciute, S. Bruckenstein, A.R. Hillman, Counter-ion specific effects on charge and solvent trapping in poly(vinylferrocene) films, J. Electroanal. Chem. 488 (2000) 73–81, https://doi.org/10.1016/S0022-0728(00)00190-X.

[85] R. Zahn, J. Vörös, T. Zambelli, Swelling of electrochemically active polyelectrolyte multilayers, Curr. Opin. Colloid Interface Sci. 15 (2010) 427–434, https://doi.org/10.1016/j.cocis.2010.07.006.
[86] W.A. Marmisollé, J. Irigoyen, D. Gregurec, S. Moya, O. Azzaroni, Supramolecular surface chemistry: substrate-independent, phosphate-driven growth of polyamine-based multifunctional thin films, Adv. Funct. Mater. 25 (2015) 4144–4152, https://doi.org/10.1002/adfm.201501140.
[87] S.E. Herrera, M.L. Agazzi, M.L. Cortez, W.A. Marmisollé, C. Bilderling, O. Azzaroni, Layer-by-layer formation of polyamine-salt aggregate/polyelectrolyte multilayers. Loading and controlled release of probe molecules from self-assembled supramolecular networks, Macromol. Chem. Phys. 220 (2019) 1900094, https://doi.org/10.1002/macp.201900094.
[88] S.E. Herrera, M.L. Agazzi, M.L. Cortez, W.A. Marmisollé, M. Tagliazucchi, O. Azzaroni, Polyamine colloids cross-linked with phosphate ions: towards understanding the solution phase behavior, ChemPhysChem 20 (2019) 1044–1053, https://doi.org/10.1002/cphc.201900046.
[89] O. Azzaroni, S. Moya, T. Farhan, A.A. Brown, W.T.S. Huck, Switching the properties of polyelectrolyte brushes via "hydrophobic collapse", Macromolecules 38 (2005) 10192–10199, https://doi.org/10.1021/ma051549r.
[90] O. Azzaroni, A.A. Brown, W.T.S. Huck, Tunable wettability by clicking counterions into polyelectrolyte brushes, Adv. Mater. 19 (2007) 151–154, https://doi.org/10.1002/adma.200601257.
[91] J. Irigoyen, S.E. Moya, J.J. Iturri, I. Llarena, O. Azzaroni, E. Donath, Specific ζ-potential response of layer-by-layer coated colloidal particles triggered by polyelectrolyte ion interactions, Langmuir 25 (2009) 3374–3380, https://doi.org/10.1021/la803360n.
[92] D.E. Grumelli, A. Wolosiuk, E. Forzani, G.A. Planes, C. Barbero, E.J. Calvo, Probe beam deflection study of ion exchange in self-assembled redox polyelectrolyte thin films, Chem. Commun. 3 (2003) 3014–3015, https://doi.org/10.1039/b308449c.
[93] Y. Marcus, Ionic radii in aqueous solutions, Chem. Rev. 88 (1988) 1475–1498, https://doi.org/10.1007/BF00646201.
[94] E.S. Forzani, M. Otero, M.A. Pérez, M.L. Teijelo, E.J. Calvo, The structure of layer-by-layer self-assembled glucose oxidase and Os(Bpy) 2 ClPyCH 2 NH−poly(allylamine) multilayers: ellipsometric and quartz crystal microbalance studies, Langmuir. 18 (2002) 4020–4029, https://doi.org/10.1021/la025507x.
[95] M. Tagliazucchi, E.J. Calvo, I. Szleifer, Molecular theory of chemically modified electrodes by redox polyelectrolytes under equilibrium conditions: comparison with experiment, J. Phys. Chem. C. 112 (2008) 458–471, https://doi.org/10.1021/jp073123f.
[96] M. Tagliazucchi, Estudio de films nanoestructurados obtenidos mediante técnicas de autoensamblado capa por capa, Tesis Dr. (2009) 2–173.
[97] G. Rydzek, Q. Ji, M. Li, P. Schaaf, J.P. Hill, F. Boulmedais, K. Ariga, Electrochemical nanoarchitectonics and layer-by-layer assembly: From basics to future, Nano Today 10 (2015) 138–167, https://doi.org/10.1016/j.nantod.2015.02.008.
[98] Y.X. Sun, K.F. Ren, J.L. Wang, G.X. Chang, J. Ji, Electrochemically controlled stiffness of multilayers for manipulation of cell adhesion, ACS Appl. Mater. Interfaces 5 (2013) 4597–4602, https://doi.org/10.1021/am401088w.
[99] R. Ahmed, S.K. Patra, L. Chabanne, C.F.J. Faul, I. Manners, Hierarchical organometallic materials: self-assembly of organic-organometallic polyferrocenylsilane block polyelectrolyte-surfactant complexes in bulk and in thin films, Macromolecules 44 (2011) 9324–9334, https://doi.org/10.1021/ma201526w.
[100] R. Ahmed, S.K. Patra, I.W. Hamley, I. Manners, C.F.J. Faul, Tetragonal and helical morphologies from polyferrocenylsilane block polyelectrolytes via ionic self-assembly, J. Am. Chem. Soc. 135 (2013) 2455–2458, https://doi.org/10.1021/ja312318d.
[101] X. Liu, N.L. Abbott, Spatial and temporal control of surfactant systems, J. Colloid Interface Sci. 339 (2009) 1–18, https://doi.org/10.1016/j.jcis.2009.07.006.
[102] T.J. Smith, C. Wang, N.L. Abbott, Redox-triggered mixing and demixing of surfactants within assemblies formed in solution and at surfaces, J. Colloid Interface Sci. 502 (2017) 122–133, https://doi.org/10.1016/j.jcis.2017.04.052.
[103] M. Naz, J. Ali, S. Fatima, S. Tabassum, S. Nawaz, A. Badshah, H. Dou, Cationic surfactants based on ferrocene containing thiourea: Synthesis, self-aggregation, and antioxidant properties, Colloids Surf. A 597 (2020), https://doi.org/10.1016/j.colsurfa.2020.124760.
[104] N. Li, S. Yi, Z. Qian, J. Wang, N. Lei, X. Chen, Multicompartment-like aggregates formed by a redox-responsive surfactant encapsulated polyoxometalate in DMF/butanol mixed solvent, RSC Adv. 7 (2017) 14631–14639, https://doi.org/10.1039/c7ra00654c.
[105] A. Andrade-Eiroa, M. Canle, V. Leroy-Cancellieri, V. Cerdà, Solid-phase extraction of organic compounds: a critical review (Part I), TrAC – Trends Anal. Chem. 80 (2016) 641–654, https://doi.org/10.1016/j.trac.2015.08.015.
[106] C. Swearingen, J. Wu, J. Stucki, A. Fitch, Use of ferrocenyl surfactants of varying chain lengths to study electron transfer reactions in native montmorillonite clay, Environ. Sci. Technol. 38 (2004) 5598–5603, https://doi.org/10.1021/es030645+.